Beam Angle Optimization for Automated Coplanar IMRT Lung Plans

by

Kathryn Hedrick

Medical Physics Graduate Program
Duke University

Date:_____
Approved:

_____
Q. Jackie Wu, Supervisor

_____
Jing Cai

_____
Anuj Kapadia

Thesis submitted in partial fulfillment of
the requirements for the degree of
Master of Science in the Graduate Program in
Medical Physics in the Graduate School
of Duke University

2016

ABSTRACT

Beam Angle Optimization for Automated Coplanar IMRT Lung Plans

by

Kathryn Hedrick

Medical Physics Graduate Program
Duke University

Date:_____
Approved:

_____
Q. Jackie Wu, Supervisor

_____
Jing Cai

_____
Anuj Kapadia

An abstract of a thesis submitted in partial
fulfillment of the requirements for the degree
of Master of Science in the Graduate Program in
Medical Physics in the Graduate School of
Duke University

2016

Abstract

Purpose: To investigate the effect of incorporating a beam spreading parameter in a beam angle optimization algorithm and to evaluate its efficacy for creating coplanar IMRT lung plans in conjunction with machine learning generated dose objectives.

Methods: Fifteen anonymized patient cases were each re-planned with ten values over the range of the beam spreading parameter, k, and analyzed with a Wilcoxon signed-rank test to determine whether any particular value resulted in significant improvement over the initially treated plan created by a trained dosimetrist. Dose constraints were generated by a machine learning algorithm and kept constant for each case across all k values. Parameters investigated for potential improvement included mean lung dose, V20 lung, V40 heart, 80% conformity index, and 90% conformity index.

Results: With a confidence level of 5%, treatment plans created with this method resulted in significantly better conformity indices. Dose coverage to the PTV was improved by an average of 12% over the initial plans. At the same time, these treatment plans showed no significant difference in mean lung dose, V20 lung, or V40 heart when compared to the initial plans; however, it should be noted that these results could be influenced by the small sample size of patient cases.

Conclusions: The beam angle optimization algorithm, with the inclusion of the beam spreading parameter k, increases the dose conformity of the automatically generated

treatment plans over that of the initial plans without adversely affecting the dose to organs at risk. This parameter can be varied according to physician preference in order to control the tradeoff between dose conformity and OAR sparing without compromising the integrity of the plan.

Dedication

This work is dedicated to Juno for loving me through all the long hours and always putting a smile on my face.

Contents

List of Tables

List of Figures

Acknowledgements

This work would not have been possible without the previous efforts and expertise of both Yang Sheng and Dr. Lulin Yuan, or the guidance of my advisor Dr. Jackie Wu.

1. Introduction

1.1 Motivation

Treatment planning for radiation therapy is an inherently complex process that involves the participation of multiple specialists. Effective treatment plans must not only deliver a prescription dose to a specified target, but also spare as much normal tissue as possible. Simultaneously an optimal plan will minimize total treatment time without compromising patient safety. As such, the input of oncologists, dosimetrists, therapists, and physicists is critical in the creation of an ideal treatment plan, but the involvement of so many professional opinions inevitably leads to a lack of consensus on what might be considered an "optimal" result or how to achieve it. This study investigates an automated treatment planning method, which would mitigate if not eliminate much of this bias.

Because of its inherent iterative nature, the treatment planning process can also take anywhere from twenty minutes to multiple hours depending on the case complexity and planner's experience. Automating this process would not only eliminate the user bias, but also be a very effective time-saving measure.

While the ultimate goal of this method is to reliably automate IMRT planning, this study aims to validate the current algorithm for selecting coplanar beam angles in lung cancer cases and compare its efficacy to that of a clinical planner.

1.2 Background

Lung cancer is the second most common cancer and the leading cause of cancer deaths in the United States, with one out of four cancer-related deaths attributable to lung cancer. The American Cancer Society predicts over 220,000 new cases of lung cancer in 2016 and anticipates over 158,000 related deaths. Five year survival rates vary wildly depending on the stage and extent of disease, but range from nearly 50% for stage I disease to only 1% for stage IV [1].

Many different treatment techniques have been proposed for treating lung cancers, varying in complexity from simple AP-PA parallel opposed fields, to 3D conformal plans and more complex intensity modulated radiation therapy (IMRT) or volume modulated arc therapy (VMAT) plans, and even stereotactic body radiation therapy (SBRT). The type of treatment depends on many factors including tumor size, location, extent, and lesion resectability [2].

1.3 Treatment Planning Overview

Intensity modulated radiation therapy (IMRT) is a treatment method that utilizes multiple beams and actively modulates the fluence of each beam during delivery through the use of a multileaf collimator (MLC). This modulation allows for better dose conformity and normal tissue sparing than conventional 3D treatment methods, especially with tumors in close proximity to critical structures. IMRT utilizes inverse planning [3].

The inverse treatment planning process begins with a 3-D patient study, usually a CT scan, to determine the size and extent of disease. The tumor and any involved critical organs can then be visualized and contoured. A prescription and dose constraints for any organs at risk (OARs) must be assigned to the structures indicated on the patient CT, at which point the planner can begin selecting beam angles to treat from. After beam placements are chosen, the planning software is used to optimize the modulation of each beam to obtain a dose distribution that most closely meets all of the indicated constraints.

The success of this optimization depends very heavily on the planning constraints used and often involves a compromise, meeting some constraints fully, others partially, and rarely others not at all. Plans are evaluated based on how well they meet the prescribed constraints and how much compromise between conflicting goals is required to do so. This is most commonly done through the assessment of isodose distributions and dose-volume histograms (DVHs), which will be described later in greater depth [4].

1.3.1 Contouring and Prescription

After a patient's initial CT or MRI scan, the target volume and any relevant organs at risk (OARs) must be indicated. The gross tumor volume (GTV) is defined as the demonstrable extent of the tumor and any involved lymph nodes. The clinical target volume (CTV) is an expansion of the GTV to include possible microscopic disease or

other areas at risk. The planning target volume (PTV) is another expansion of the volume to account for internal motion of the tumor, errors in patient setup, and any other alignment uncertainties. The OARs can also be expanded to create a planning risk volume (PRV) with an additional margin of avoidance [3].

The prescription dose specified by the oncologist is prescribed to the PTV, ensuring that the tumor will fall within the region receiving the intended dose despite any potential internal motion or alignment errors. However, because the PTV must be larger (sometimes considerably so) than the tumor itself it can be difficult to spare critical structures if they are located close to the tumor. Figure 1 shows an example where the contoured PTV (red) clearly overlaps with the heart (pink). This challenge is mitigated by the use of IMRT, because the addition of beam modulation allows for more conformal dose distributions than classical 3-D conformal treatments [3].

Figure 1: Example of CT contours - spinal cord (green), esophagus (orange), heart (pink), and PTV (red).

Prescription doses for lung cancer vary with diagnosis, intent (either curative or palliative), and stage. In general, the goal is to deliver at least 60 Gy to any gross disease. Post-operative doses to tend to be in the region of 50 Gy, with a boost of 54-60 Gy to any positive margins. Tumors in the mediastinum are typically treated with lower doses of 40-45 Gy [2].

1.3.2 Beam Angle Selection

Choosing the appropriate beam angles is largely a function of patient anatomy. By utilizing the beam's eye view (BEV) feature in the treatment planning software, contoured structures can be viewed in a plane perpendicular to the central axis of the

potential beam direction as demonstrated by Figure 2. Preferred beam angles generally take advantage of greater separation between the target volume and adjacent OARs [3].

The number of beams used also plays a role in the efficacy of a treatment plan. Generally, more beams provide better dose homogeneity and OAR sparing. However, increasing the number of beams also increases the time required for both dose optimization and treatment delivery, so copious numbers of beams should be avoided [4].

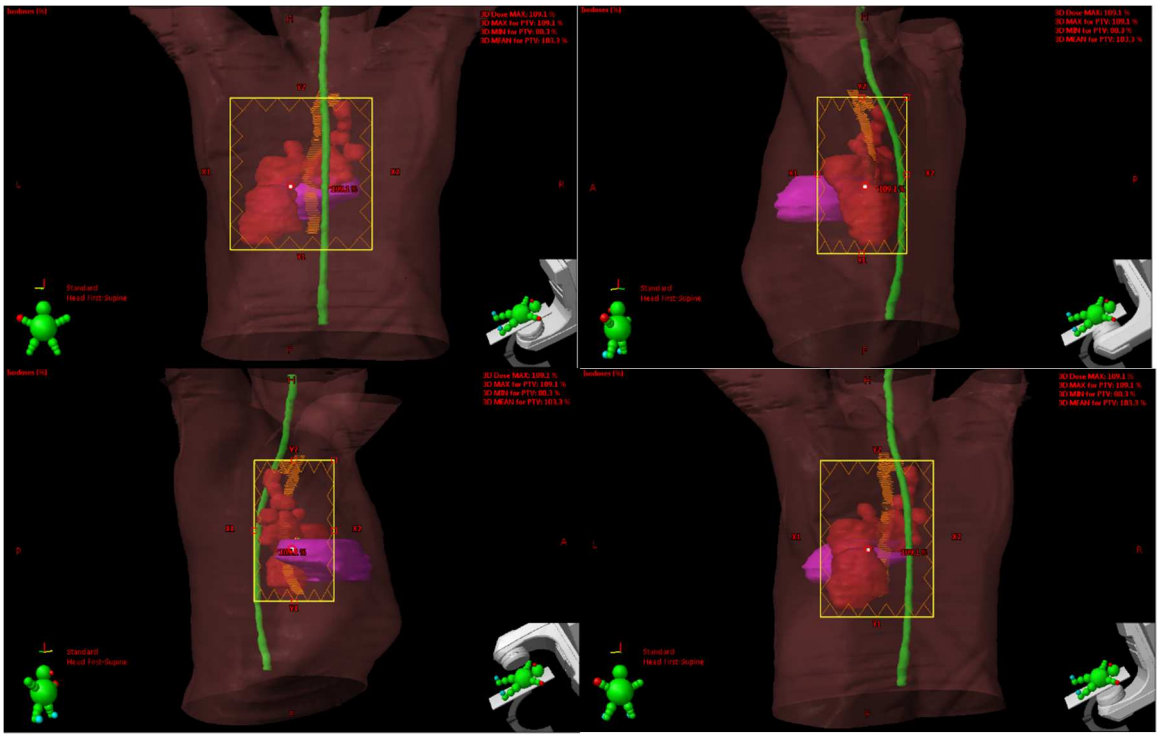

Figure 2: Example of structures visualized via the BEV tool from multiple angles (contours - spinal cord (green), esophagus (orange), heart (pink), and PTV (red)).

For some treatment sites where differences in patient anatomy are minimal (such as prostate), standard templates can be used. However, for treatment sites where patient

anatomy is more variable (such as head and neck or lung), the beam arrangement depends heavily on the structure geometry and planner experience [5].

1.3.3 Dose Constraints and Optimization

In order to both maximize PTV coverage and minimize irradiation of normal tissues, dose constraints must be chosen to input into the optimization software. The Quantitative Analysis of Normal Tissue Effects in the Clinic (QUANTEC) outlines recommended dose-volume limits and their associated endpoints [6]. While ideally the dose to OARs should be as low as possible, QUANTEC provides data which is often used as a starting point for selecting dose constraints or as a final check that a plan meets all requirements to ensure patient safety and minimizes the risk of future complications. Relevant dose constraints specifically for lung plans are discussed in depth later in section 2.4.

Figure 3 illustrates how dose constraints are specified in the treatment planning software. Constraints can either be entered numerically as a dose-volume condition or placed graphically on the intermediate plan DVH. Each constraint must also be assigned a priority for optimization.

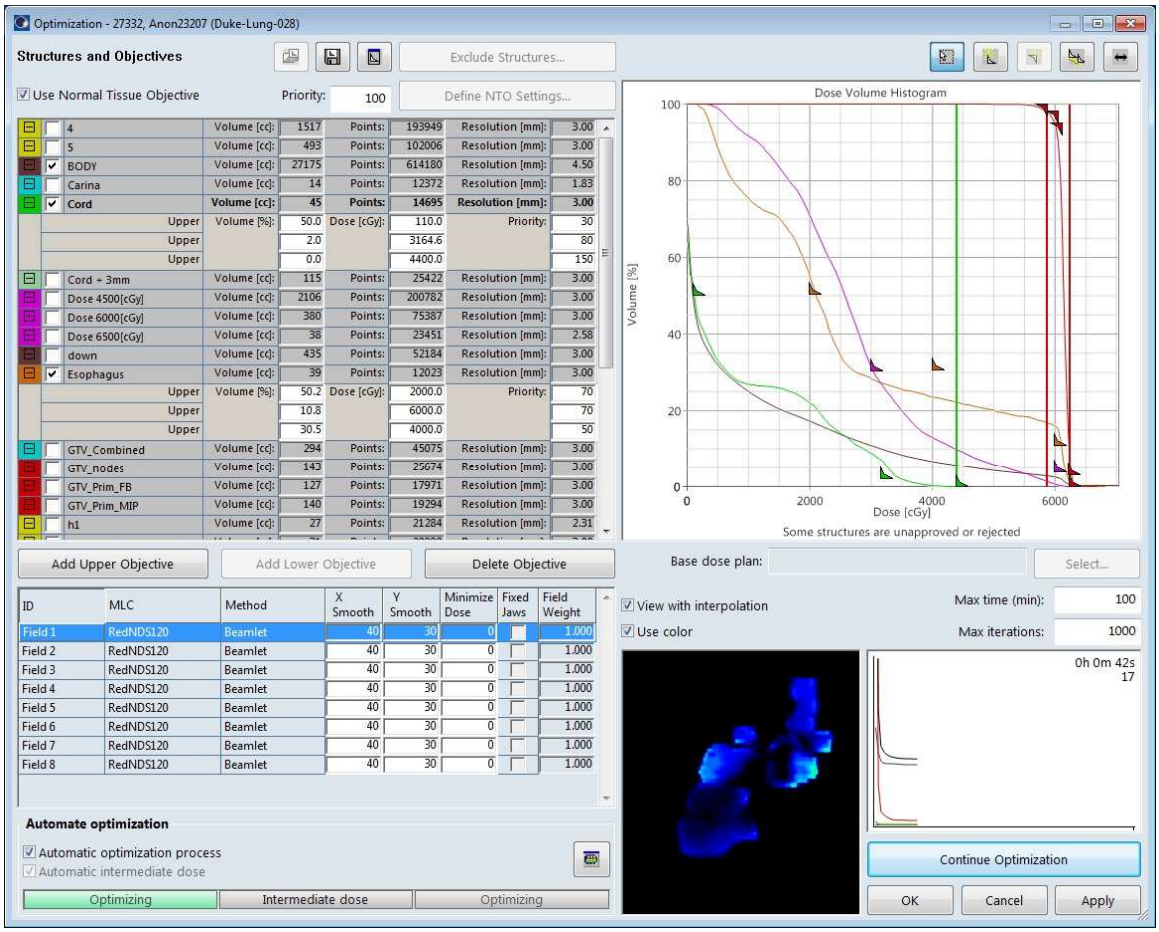

Figure 3: The plan optimization window in Eclipse, depicting the dose constraints overlaid on the intermediate plan DVH.

The treatment planning software utilizes an algorithm with two major functions to optimize the fluence of each beam. The objective function characterizes violations of the dose constraints and assigns a score to the plan at each iteration. Equation 1 shows an example target objective function that uses an average weighted sum of squared differences between the prescribed and delivered doses over all involved voxels. It should be noted that these equations (Equations 1 and 2) are provided purely for

illustrative purposes and are not representative of the considerably more complex algorithms used by the treatment planning system [5].

$$\mathbf{\Omega^{target}} = \boldsymbol{w_{max}^{target}} \times \sum\left(\frac{\max\left(d_i^{target} - d_{max}^{target}, 0\right)^2}{N_{target}}\right) + \boldsymbol{w_{min}^{target}} \times \sum\left(\frac{\max\left(d_{min}^{target} - d_i^{target}, 0\right)^2}{N_{target}}\right) \qquad \mathbf{1}$$

This particular objective function would assign penalties if a target voxel dose was less than d_{min}^{target} or greater than d_{max}^{target}, but not if the dose falls into the allowed range specified by these values. The priority assigned to both the minimum and maximum dose constraint is denoted by w, which can be varied by the planner.

Objective functions are also used to characterize the allowed doses to OARs and assign penalties accordingly. An example constraint objective function is shown in Equation 2 [5].

$$\mathbf{\Omega^{constraint}} = \boldsymbol{w_{min}^{constraint}} \times \sum \frac{\max\left(d_{min}^{constraint} - d_i^{constraint}, 0\right)^2}{N_{constraint}} \qquad \mathbf{2}$$

The total objective function is the sum of all constituent objective functions, which is used in the next step.

The second major function employed by the treatment planning software during optimization is an iterative process than attempts to minimize the values of the objective functions by adjusting the beam fluences. Because it is rarely possible to create a plan that meets all of the constraints, the planner must assign a priority weight to each constraint so that the software is able to find an appropriate compromise when necessary [5].

After each iteration, the intermediate DVH shown in Figure 2 will be updated to reflect the current state of optimization. The number of required iterations and total optimization time vary depending on the number of beams and strictness of the objectives. Overly restrictive or lenient objectives may also result in an inferior plan because the software will either assign extreme fluences values in order to meet impossible objectives or meet lax objectives and finish optimizing before the ideal result is found [5].

1.3.4 Plan Evaluation

Completed plans are generally evaluated on how well they both spare OARs and deliver prescription dose to the PTV. Two common ways to visualize these aspects of a plan are isodose distributions and dose-volume histograms. Isodose lines are superimposed on the CT data set in the planning software. This method is most effective for identifying and locating regions of particularly high or low dose and illustrating both the conformity and homogeneity of the dose to the target [4].

Figure 4 shows isodose lines superimposed on a patient CT scan. The 100% prescription isodose line shown in white clearly encompasses the PTV in the left lung, and allows for qualitative analysis of dose conformity and OAR sparing.

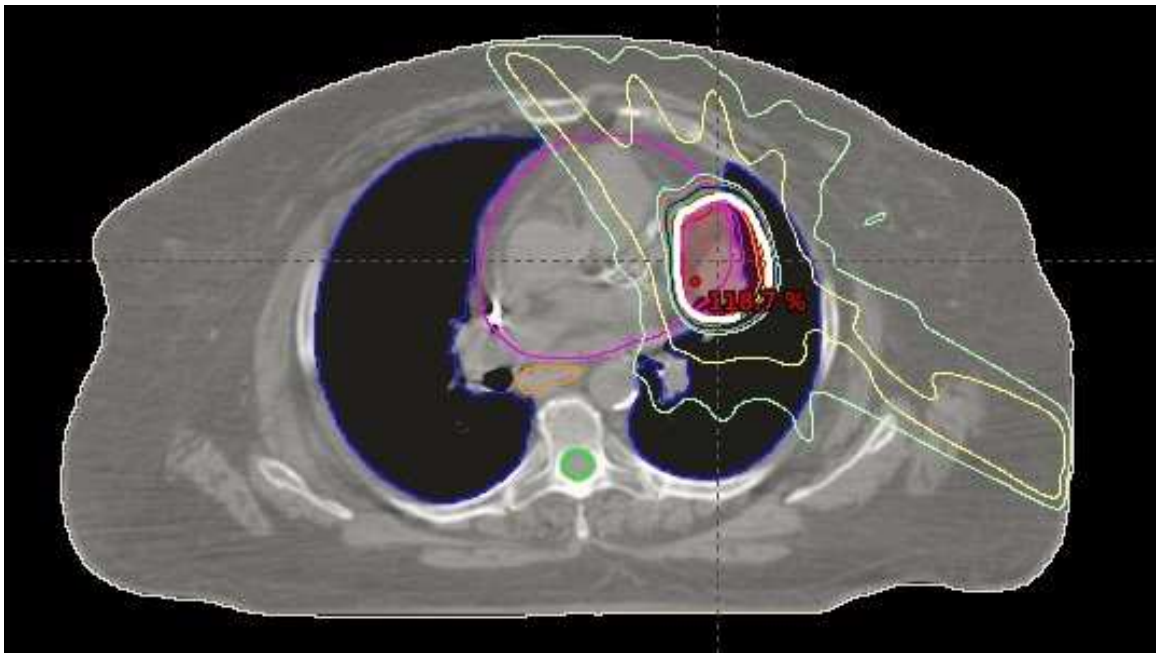

Figure 4: Example isodose lines superimposed on a treatment plan (contours – spinal cord (green), esophagus (orange), and PTV (red)).

Whereas the inspection of isodose lines is largely qualitative, examining the plan's DVH allows for a more quantitative analysis. As shown in Figure 5, the DVH is a plot of structure volume vs. dose, incorporating the PTV and all OAR doses into a single figure. Because the DVH is also used during the optimization phase to depict dose constraints (Figure 3), it is an especially useful quality check for planners and oncologists [3].

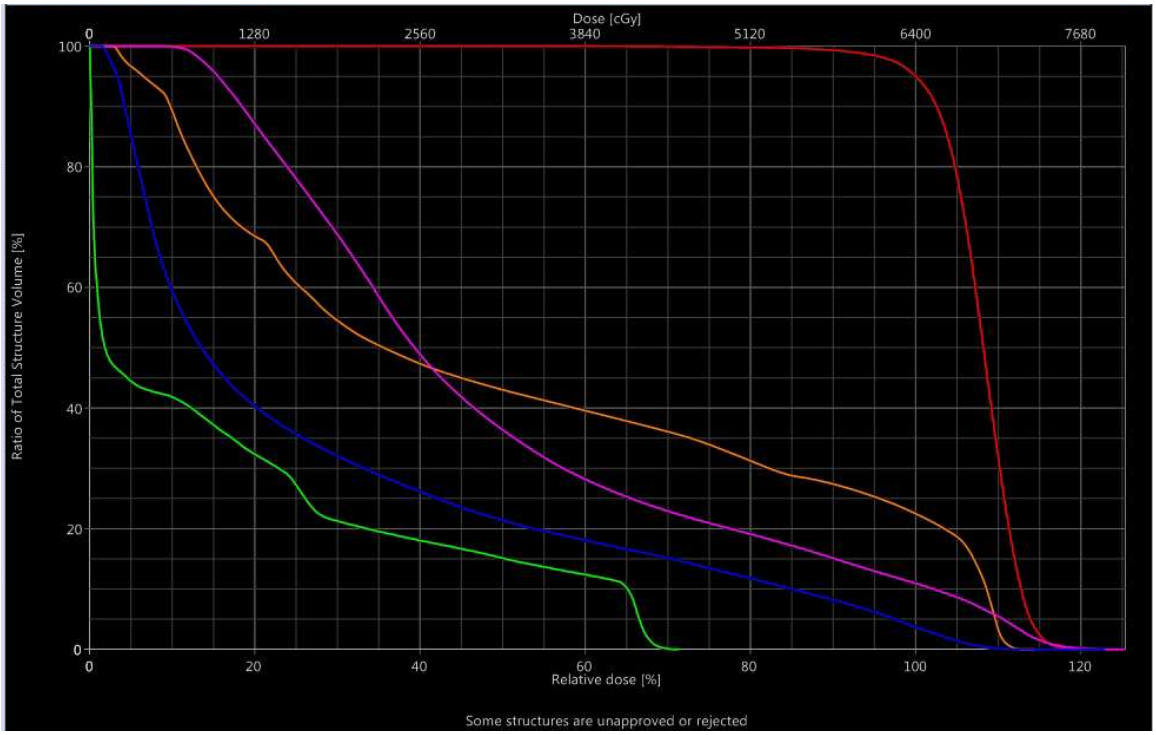

Figure 5: Example dose-volume histogram showing relevant contours – spinal cord (green), esophagus (orange), heart (pink), and PTV (red).

1.4 Previous Work

1.4.1 Automated Beam Angle Selection

Numerous studies to investigate automated selection of beam angles for IMRT planning have been conducted in the past [7-12]. These studies used a wide variety of optimization methods, including simulated annealing [7], genetic algorithms [9], sparse optimization [11], and nested partition methods [12]. Unfortunately, these global optimization processes are iterative and time consuming. To combat this, another study employed a process which either added or eliminated beams sequentially rather than

searching for an optimal arrangement all at once [13]. Still other studies relied on scores assigned to candidate beam angles based on doses delivered to the PTV and OARs along the beam path [14, 15], by using cluster analysis to choose between two prepopulated beam arrangements [16], or by separating cases into classes based on tumor location and assigning the most frequently used arrangement for each class [17]. In this work, the beam angle selection is determined by analysis of patient-specific anatomy via a weighted path length comparison along potential beam angles.

1.4.2 Automated Dose Constraint Selection

Operating on the premise that high-quality prior plans can be used to guide current planning practices on similar patient sets, an additional study investigated the sources of interpatient variation in DVH curves. A support vector regression model was trained to map extracted anatomical features from PTVs and OARs of these prior plans to corresponding dose-volume features. The model was then used successfully to predict obtainable DVHs of OARs in several new cases [18]. This DVH prediction model was adapted to select the dose constraints in this work.

2. Methods and Materials

Fifteen anonymized patient lung cases previously treated with IMRT were used to evaluate the efficacy of the beam angle selection algorithm. Of these cases, five each had tumors located in the left lung, right lung, and mediastinum. Dosimetric properties of the resulting plans were then compared to the original clinically delivered plans.

2.1 Planning Overview

The IMRT plans were created using a combination of two methods, one which created the dose-volumes objectives and another which selected the beam angles, as shown below in Figure 6. The upper portion of the figure involves modeling with other patient sets from previous works (see section 1.4), whereas this study mostly involves the patient-specific tasks outlined in the lower portion.

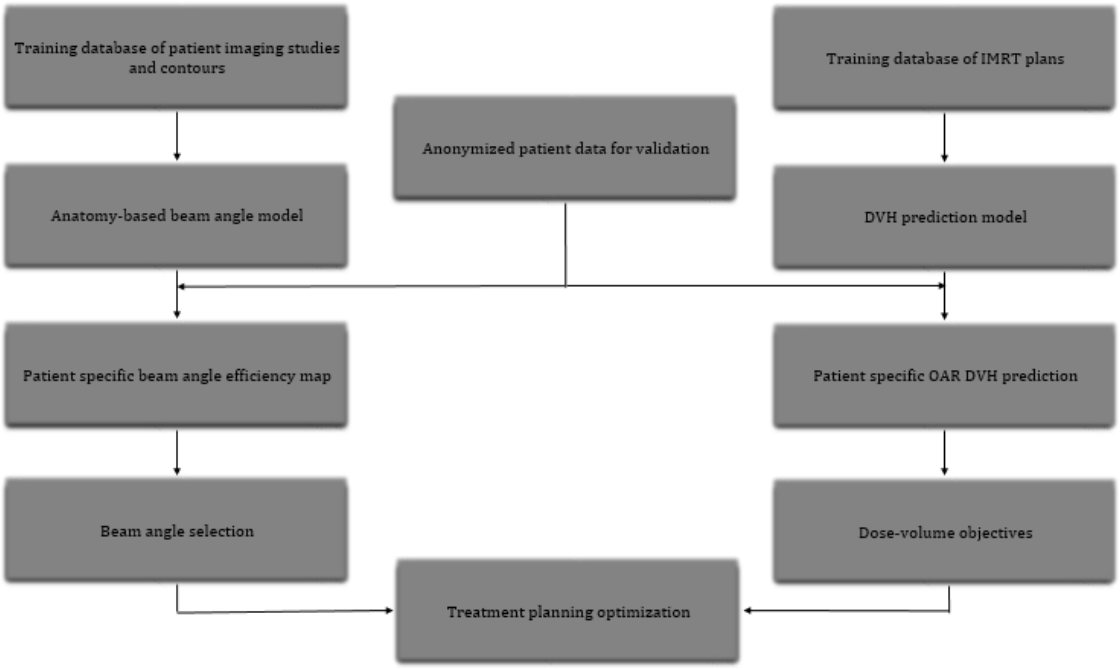

Figure 6: Flowchart indicating various elements of plan automation.

The dose-volumes objectives were chosen based on DVH prediction models trained with previously treated IMRT lung plans [18]. A single template was generated for each patient case and was left unchanged as other parameters were varied.

The second method which selects the beam angles is the main focus of this work. Beam efficiency indices are calculated from the patient CT and contours by using a weighted ratio of OAR to PTV path length for each candidate beam. Unlike previous work using this algorithm, for this study an additional term was included to modify the spreading between the individual beams as well. As the focus of this work, this parameter (k) was varied from 0.1 to 1.0 in increments of 0.1, in an effort to determine whether an ideal value exists.

2.2 Beam Efficiency Index Map

The ray efficiency index is defined in Equation 3 where w indicates the weighting for each structure and d indicates the doses delivered to each structure along the beam path.

$$\boldsymbol{q_{av}} = \frac{\sum(\boldsymbol{w_{structure}} * \boldsymbol{d_{structure}})}{\max(\boldsymbol{d_{PTV}}, \mathbf{0.8})} \qquad \mathbf{3}$$

The structures included in the calculation are the OARs (heart, esophagus, spinal cord, liver, stomach, kidney, and lung), normal tissues, and the PTV. Both dose attenuation and lung tissue inhomogeneity were accounted for in the dose calculation. The OAR and PTV weighting were kept constant for all plans.

This index is calculated for each potential ray path originating in a voxel v with direction a. In order to simulate a beam passing through the patient rather than a ray (as the path length comparison in Equation 3 implies) the indices for the same direction (a) that intersect the PTV were averaged to create the beam efficiency index defined in Equation 4 below.

$$\boldsymbol{EI(a)} = \sum_{\boldsymbol{v \in PTV}} (\boldsymbol{q_{av}}) \qquad \mathbf{4}$$

The indices of these beams can then be visualized as a rose diagram as shown in Figure 7, henceforth referred to as the beam angle efficiency map. Because lower values of the efficiency index correspond to a more favorable ratio of OAR and PTV dose, smaller radii on the efficiency map indicate more optimal beam orientations.

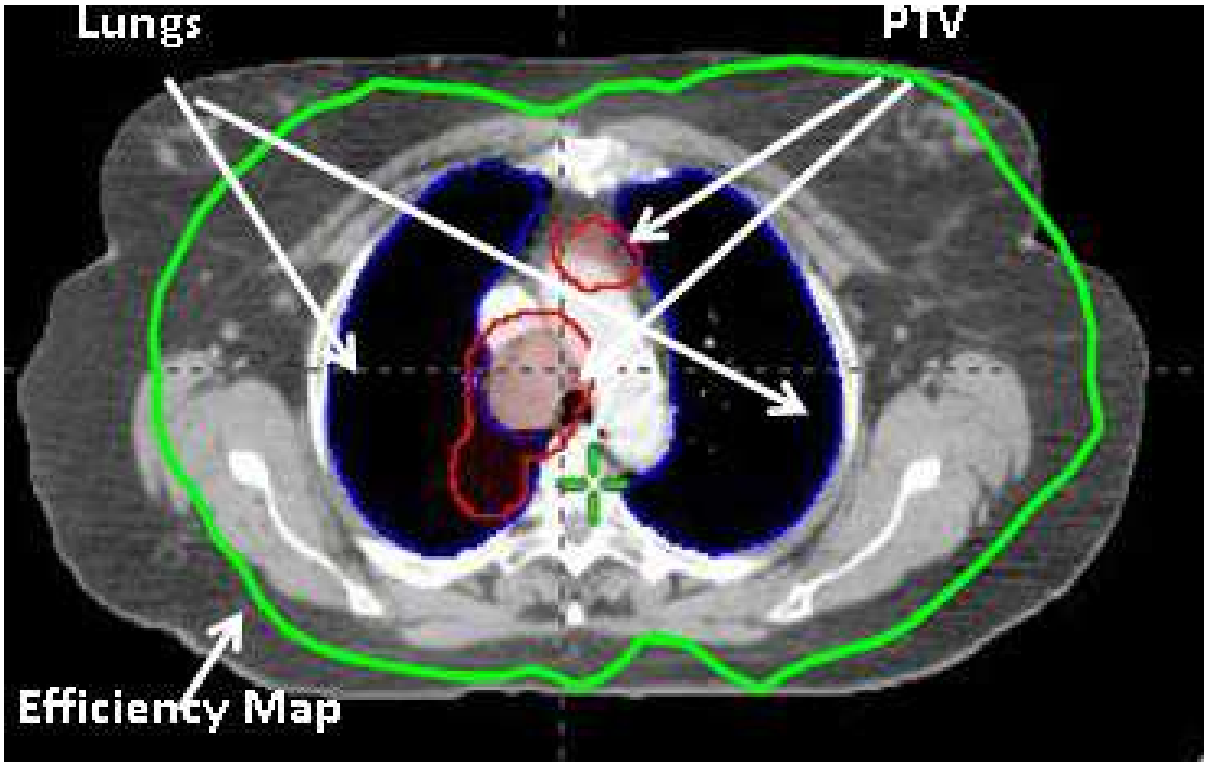

Figure 7: Example beam efficiency index map.

In this study, an additional term was added to the beam efficiency index to allow the user to adjust the beam separation. With the previously defined index (Equation 4), the algorithm had a tendency to place multiple beams in the concave areas of the map resulting in excessive hot spots and high skin doses. The new efficiency index is defined as follows

$$\boldsymbol{EI} = \boldsymbol{EI}(\boldsymbol{a}) + \sum_{i \neq j} \left(\frac{k}{1 - \cos a_{ij}} \right) \qquad \mathbf{5}$$

where k represents the relative importance of beam separation. Increasing this value will increase the beam spreading at the expense of increasing the value of the efficiency index; however, this effect is limited by the patient anatomy. Figure 8 shows the effect that changing k has on the beam angle distribution for an example case.

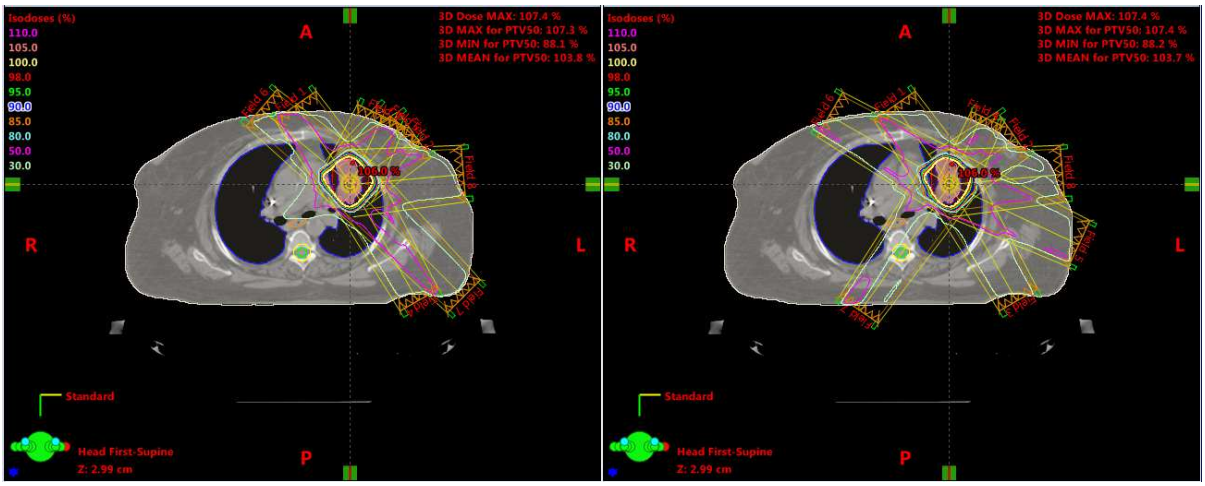

Figure 8: Effect of varying *k* value on field distribution for favorable anatomy, minimum value shown on left and maximum value shown on right.

Since *k* is a relative measure that competes with the anatomy-dependent term of the efficiency index, for some patient anatomies and tumor locations varying the value of *k* has limited effect. In these cases (commonly when the tumor is present in the mediastinum), the anatomy-dependent term dominates the efficiency index and field distributions for various *k* values are similar or identical as shown in Figure 9 on the next page.

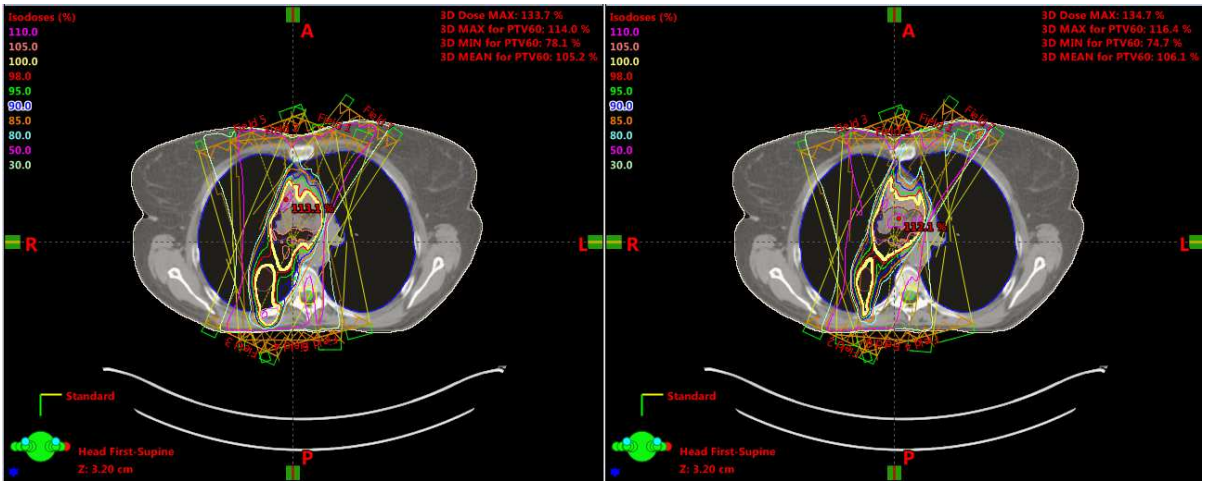

Figure 9: Effect of varying *k* value on field distribution for non-favorable anatomy, minimum value shown on left and maximum value shown on right.

2.3 Partially Automated IMRT Planning

The beam angle selection algorithm generates plan templates that can be imported directly into the Eclipse treatment planning system. For comparison purposes, all plans were replanned using eight beams and then normalized to a nominal prescription of 64 Gy, with 100% of this dose covering 95% of the PTV. For each of the fifteen patient cases, ten values of *k* were used (ranging from 0.1 to 1.0 in increments of 0.1) for a total of 150 new plans.

Figure 10 below shows the beam angle optimization user interface. Priorities for OAR avoidance can be specified as well as the beam separation parameter *k* and a number of allowable non-coplanar angles. For this study, all algorithm-generated plans were created using exclusively coplanar beams. After running for a particular case, the interface will

display the beam angle efficiency map for the PTV (cyan), lungs (pink), and combined body (blue) on the left as well as plot the selected beam angles on the right.

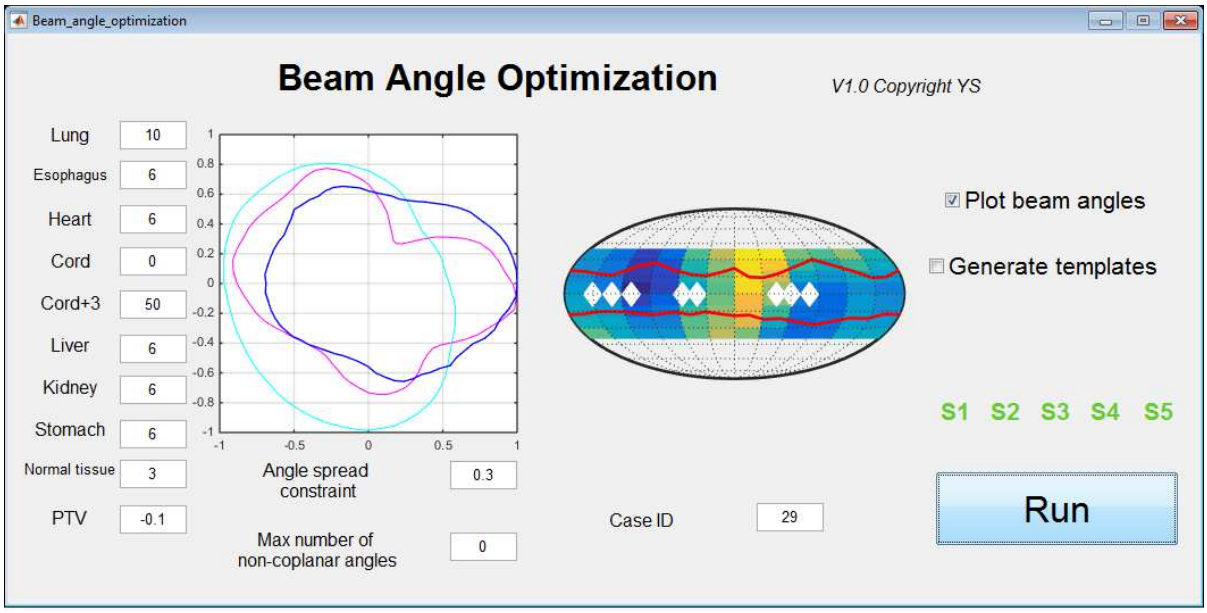

Figure 10: Beam angle optimization user interface, showing efficiency map and beam angle plot.

The machine learning component that selects the dose constraints also generates templates for use in optimization. These templates are generated on a per case basis and were left unchanged during the optimization and while varying the value of k for each patient.

While not completely automated, this process drastically reduces the time it takes to create a plan, minimizes the necessary user input, and eliminates the often iterative process of selecting beam angles.

2.4 Parameters Used for Analysis

In order to evaluate the efficacy of the automated planning method and the beam angle optimization algorithm specifically, several parameters were chosen to characterize the results. Because the major challenge in treatment planning is balancing the trade-off between OAR sparing and PTV dose coverage, both dosimetric parameters for critical structures and conformity indices were selected. To characterize OAR sparing, the mean lung dose, the volume of the lungs receiving 20 Gy or more (V20 lung), and the volume of the heart receiving 40 Gy or more (V40 heart) were chosen, because the endpoints for the lung and heart are potentially the most severe of the involved OARs.

The mean lung dose, V20 lung, and V40 heart should all ideally be minimized during treatment planning. Numerous QUANTEC papers have been published on the subject of lung and heart dose-volume effects and endpoints [6, 19, 20]. When considering the lung, the endpoint of interest is symptomatic radiation pneumonitis, which occurs in between 5-50% of lung patients. The risk of developing radiation pneumonitis has been found to increase with delivered dose. Specifically, limiting the mean lung dose to 20-23 Gy and V20 lung to 30% has been found to reduce the risk of radiation pneumonitis to less than 20% [19].

When considering the heart, the endpoints range from pericarditis to more serious late injuries such as congestive heart failure, ischemia, coronary artery disease, and myocardial infarction. It has been noted that in the treatment of certain cancers, radiation-

induced heart disease is a leading cause of mortality. QUANTEC guidelines suggest limiting V25 to 10% (associated with a 1% risk of cardiac mortality) but this was obtained using an overly conservative model [20]. Other studies on the subject indicate that V40 has a strong correlation with long-term cardiac mortality and should be limited to less than 50% [21, 22]. All three of these parameters should be minimized during the treatment planning process, so lower values for the algorithm-generated plans than the initial plans would indicate improvement.

To characterize high dose conformity, 80% and 90% conformity indices were selected. The conformity index for a given isodose value is defined as the volume enclosed by that isodose level divided by the target volume, as shown below in Equation 6.

$$\boldsymbol{C_{isodose} = \frac{V_{isodose}}{V_{target}}} \qquad \mathbf{6}$$

An index of less than one indicates under-dosing of the target, whereas an index of greater than one indicates over-dosing of the target and/or adjacent normal tissues. Because all of the conformity indices measured in this study were greater than one, lower values for the algorithm-generated plans than the initial plans indicate improvement.

2.5 Wilcoxon Signed-Rank Test

The newly generated plans were compared to the original clinically treated plan with a series of Wilcoxon signed-rank tests in Matlab. Similar to a paired t-test, this test determines whether two datasets share a mean; however, unlike a paired t-test, the Wilcoxon signed-rank test does not require the datasets to be normally distributed, which

makes it ideal for comparing the dosimetric parameters gathered from the automated plans. The Matlab function *signrank* was used to compare the mean lung dose, V20 lung, V40 heart, and conformity indices at eighty and ninety percent with a 5% confidence level.

All parameters were compared using a two-sided test, which specifically tested whether the dosimetric values from the new plans were significantly different than those of the originals. If those tests passed for a particular parameter, a single-sided test was then used to verify whether the change reflected an improvement or detriment compared to the original plans.

3. Results

3.1 Analysis of All Plans

Table 1 below summarizes the dosimetric data of all the algorithm-generated plans separated by *k* value. The data from the original fifteen patient plans is included at the top and the average of all algorithm-generated plans is included at the bottom for reference.

Table 1: Mean ± standard deviation (and p-values) for all dosimetric parameters and values of *k* for all cases (significance level = 0.05).

k Value	Mean Lung Dose (cGy)	V20 Lung (%)	V40 Heart (%)	80% Conformity	90% Conformity
Initial	1268.2 ± 390.4	22.0 ± 8.0	9.6 ± 8.3	2.5 ± 0.7	1.9 ± 0.5
0.1	1234.2 ± 455.3 (0.330)	30.0 ± 10.5 (0.421)	12.1±14.9 (0.831)	2.3 ± 0.8 (0.036)	1.8 ± 0.5 (0.028)
0.2	1248.4 ± 456.8 (0.389)	22.1 ± 10.8 (0.421)	8.8 ± 8.4 (0.465)	2.1 ± 0.5 (0.005)	1.6 ± 0.3 (0.001)
0.3	1266.1 ± 466.4 (0.762)	23.0 ± 11.4 (1.000)	9.0 ± 9.2 (0.470)	2.1 ± 0.5 (0.013)	1.6 ± 0.3 (0.002)
0.4	1284.8 ± 465.1 (1.000)	23.4 ± 11.4 (0.489)	9.0 ± 8.8 (0.305)	2.1 ± 0.5 (0.004)	1.6 ± 0.3 (0.001)
0.5	1299.5 ± 481.3 (0.720)	24.3 ± 12.2 (0.229)	9.1 ± 8.6 (0.340)	2.1 ± 0.5 (0.009)	1.6 ± 0.3 (0.001)
0.6	1306.6 ± 491.9 (0.599)	24.4 ± 12.4 (0.277)	10.1 ± 10.3 (0.454)	2.1 ± 0.5 (0.009)	1.6 ± 0.3 (0.001)
0.7	1309.2 ± 492.2 (0.421)	24.5 ± 12.4 (0.208)	10.2 ± 10.3 (0.497)	2.1 ± 0.5 (0.008)	1.6 ± 0.3 (0.001)
0.8	1310.7 ± 491.3 (0.389)	24.6 ± 12.4 (0.169)	10.6 ± 11.0 (0.542)	2.1 ± 0.5 (0.008)	1.6 ± 0.3 (0.001)
0.9	1313.0 ± 495.7 (0.489)	24.9 ± 12.6 (0.121)	10.5 ± 11.1 (0.622)	2.1 ± 0.5 (0.013)	1.6 ± 0.3 (0.001)
1.0	1313.1 ± 494.1 (0.489)	24.9 ± 12.5 (0.107)	10.6 ± 11.1 (0.622)	2.1 ± 0.5 (0.013)	1.6 ± 0.3 (0.001)
Average	1288.6 ± 465.4	23.8 ± 11.6	10.0 ± 10.2	2.1 ± 0.5	1.6 ± 0.3

As will be discussed in more depth in the following sections, Table 1 shows that only the 80% and 90% conformity indices have significant p-values which indicate a statistically

measureable improvement of the algorithm-generated plans over the initial plans (11% and 13% improvements respectively). The other three dosimetric parameter results are not significant, indicating that the distribution of values is statistically similar to that of the initial plans. Both the mean lung dose and V20 lung appear to have some correlation with the beam separation parameter k, whereas V40 heart does not.

3.1.1 Percent Difference Plots

Although all of the algorithm-generated plans were normalized to the same prescription dose to obtain the dose and volume measurements in Table 1, variations in patient anatomy lead to drastically different values for the dosimetric parameters (as evidenced by the large standard deviations), making it difficult to meaningfully compare results. Therefore, in order to visualize the results from multiple cases on a single plot, the percent differences from the initial plans were used instead of the raw values.

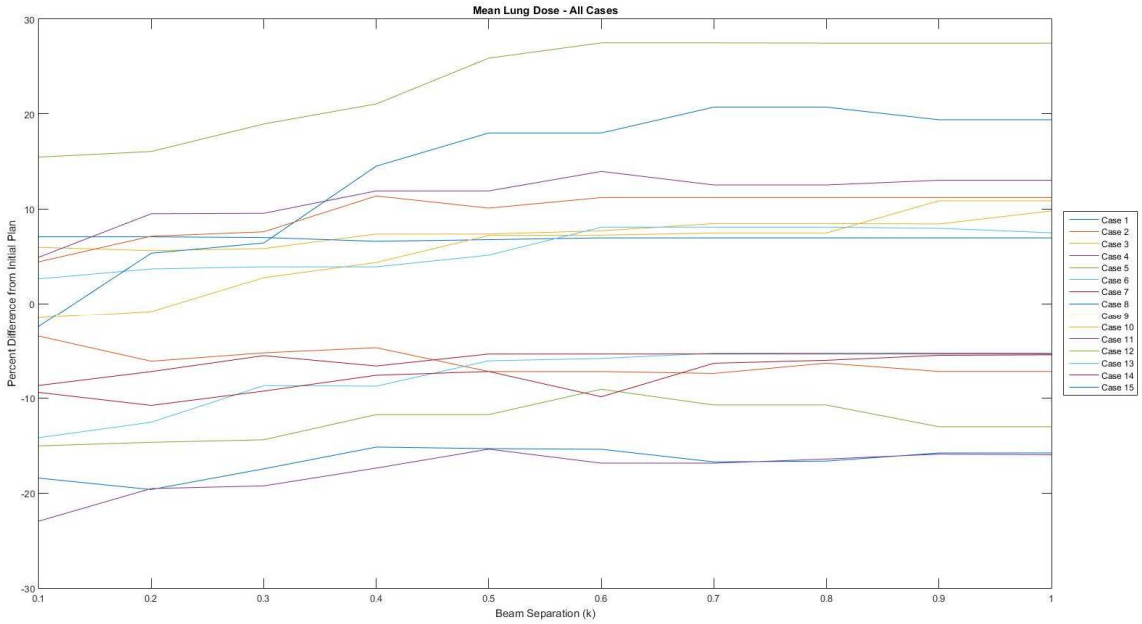

Figure 11: Mean lung dose as a function of *k* for all patient cases.

The mean lung dose shown in Figure 11 appears to have a very loose, positive correlation with the *k* value, but because the cases are centered about zero (which indicates the value of the initial plan since the results are plotted as percent differences) the distribution of mean lung dose measurements for any particular value of *k* does not seem to differ from the distribution of original plans. However, it can be inferred from the above plot that generally speaking for a given case increasing the beam separation will slightly increase the mean lung dose.

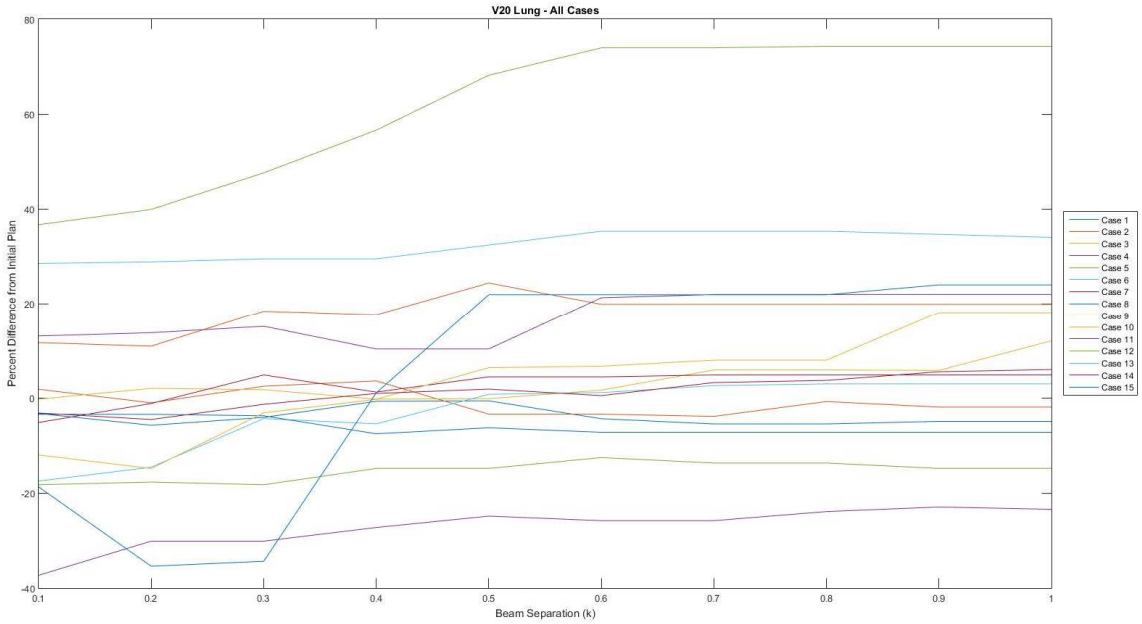

Figure 12: Volume of the lungs receiving 20 Gy or more as a function of *k* for all patient cases.

The value of V20 lung shown in Figure 12 displays similar variation to the mean lung dose. In fact, as one would expect, the cases with the greatest variation in mean lung dose also show large variations in V20. Also like the assessment of mean lung dose, the distribution of V20 lung was found to center around zero, indicating little if any difference from the distribution of initial plans.

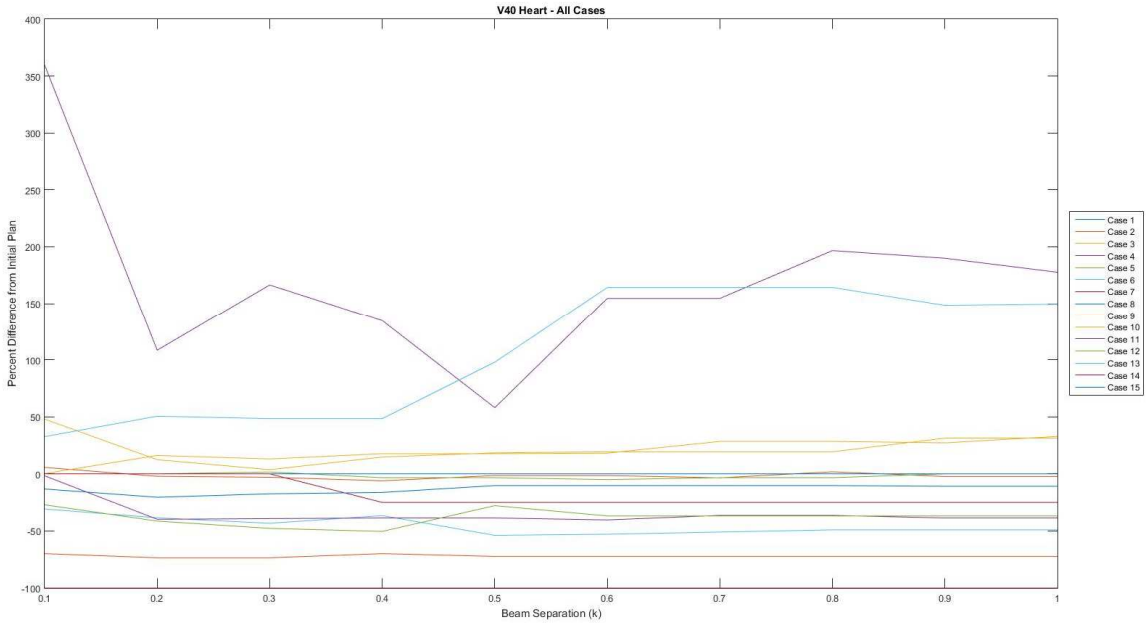

Figure 13: Volume of the heart receiving 40 Gy or more as a function of *k* for all patient cases.

The value of V40 heart shown in Figure 13 displays drastically more case-to-case variation that the previous parameters, with dose reductions up to 100% in one case and increases of over 300% in another. When eliminating these clear outliers though, the distribution of cases is yet again clustered about zero, which indicates that the algorithm-generated plans and initial plans show similar distributions of this parameter.

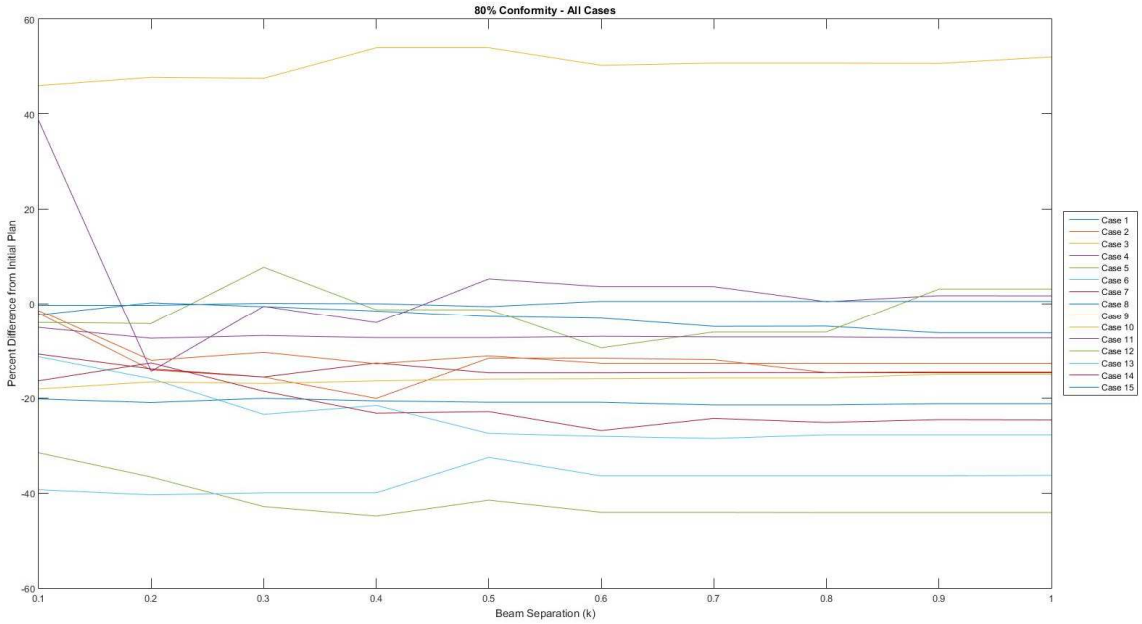

Figure 14: Conformity of 80% prescription dose as a function of *k* for all patient cases.

Unlike the previous parameters, the 80% conformity index shown in Figure 14 reveals that the cases are distributed not about zero, but about -11%. This implies that the algorithm-generated plans have 80% conformity indices that are noticeably better than the initial plans, which was confirmed earlier by the signed-rank test.

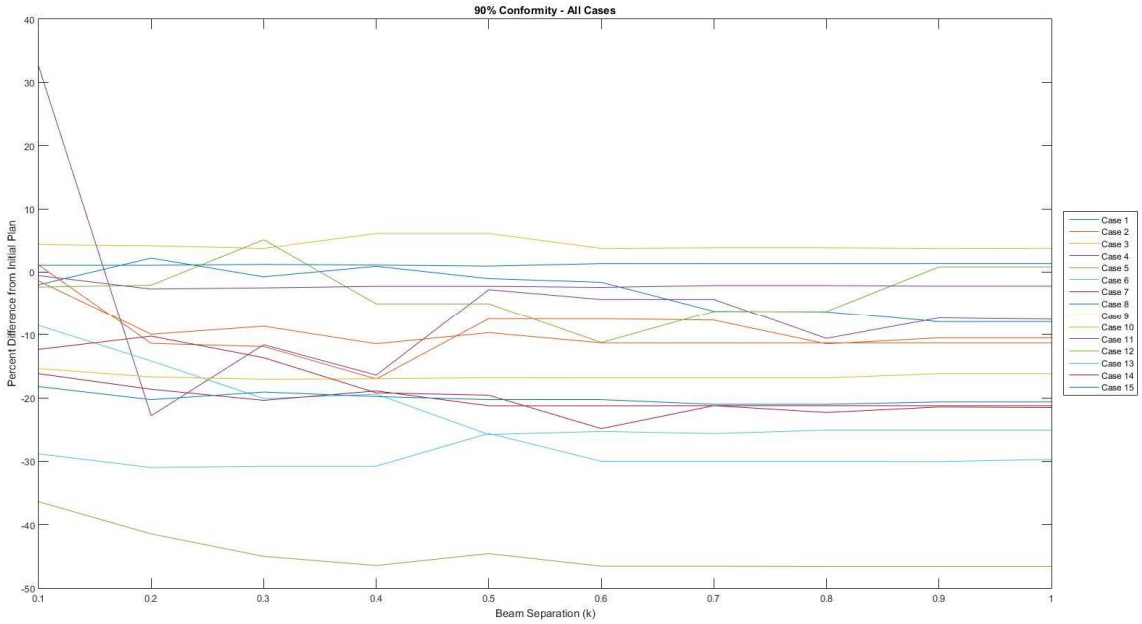

Figure 15: Conformity of 90% prescription dose as a function of *k* for all patient cases.

Similar to the 80% conformity index, the 90% conformity index shown in Figure 15 also depicts a clustering of cases with a clearly non-zero mean, approximately -13%. Similar to the previous conformity index, the mean percent difference is negative and the p-values from the signed-rank test in Table 1 confirm that these results from the algorithm-generated plans correspond with a significant improvement over the initial plans.

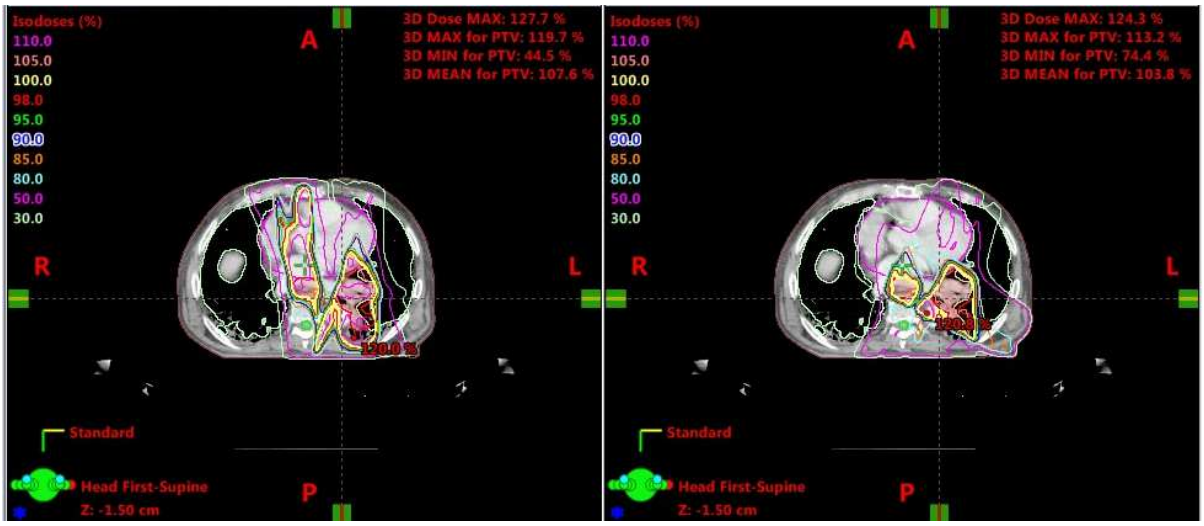

Figure 16: A comparison of dose conformity between the initial plan (left) and the algorithm-generated plan (right).

Above, Figure 16 illustrates how this improvement in conformity translates into 3D dose distribution. The 100% isodose line shown in yellow clearly conforms better to the PTV in the algorithm-generated plan (pictured at right) than in the initial plan (pictured at left). A DVH comparison of the two plans, shown below in Figure 17, also depicts an increase in PTV dose homogeneity. The curves representing PTV dose for both plans are plotted simultaneously. The algorithm-generated plan denoted by the square points has a markedly steeper dose gradient than the initial plan denoted by the triangular points. A steeper dose gradient is desirable for the PTV dose, because more of the target is receiving the prescription dose (64 Gy) while less of the target is being over-dosed.

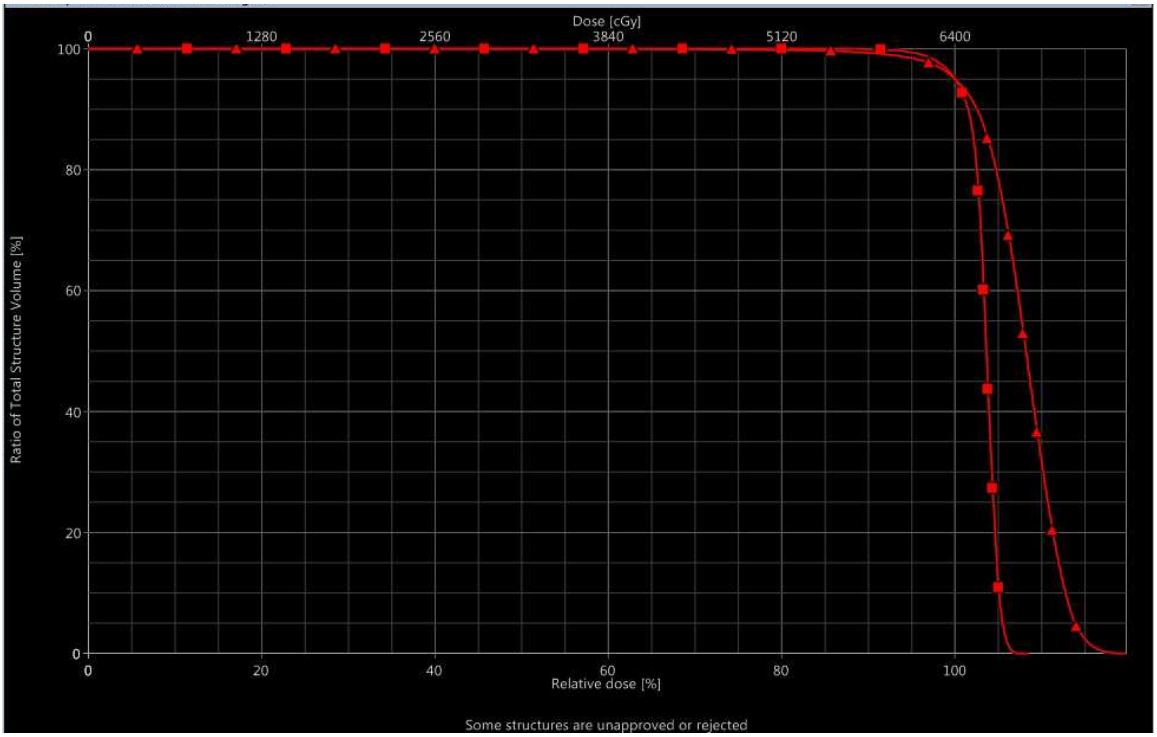

Figure 17: DVH comparison between the initial plan (triangles) and the algorithm-generated plan (squares).

3.2 Characterization of Tumor Location

Once significant differences in the mean lung dose, V20 lung, and V40 heart were rejected by the signed-rank test, the patient cases were reinvestigated in smaller groups to assess whether trends existed based on tumor location. There were five cases each where the tumor was in the left lung, right lung, and mediastinum. Because of this small sample size, the results are reported here in tabular form rather than plotted.

Table 2: Mean ± standard deviation (and p-values) for all dosimetric parameters and values of *k* for left lung cases (significance level = 0.05).

k Value	Mean Lung Dose	V20 Lung	V40 Heart	Conformity (80%)	Conformity (90%)
Initial	1320.8 ± 429.3	23.3 ± 8.6	13.0 ± 11.2	2.6 ± 0.7	2.0 ± 0.5
0.1	1302.6 ± 556.1 (0.813)	23.0 ± 12.8 (0.438)	22.1 ± 22.2 (0.375)	2.4 ± 1.0 (0.688)	1.8 ± 0.6 (0.313)
0.2	1310.7 ± 555.8 (0.813)	23.3 ± 12.8 (0.813)	13.9 ± 11.2 (0.625)	2.1 ± 0.4 (0.313)	1.5 ± 0.2 (0.063)
0.3	1337.3 ± 580.3 (1.000)	24.7 ± 14.1 (1.000)	14.6 ± 12.9 (0.625)	2.1 ± 0.5 (0.313)	1.6 ± 0.3 (0.063)
0.4	1361.4 ± 589.8 (1.000)	25.6 ± 15.1 (1.000)	14.2 ± 12.1 (1.000)	2.1 ± 0.5 (0.313)	1.5 ± 0.2 (0.063)
0.5	1393.8 ± 623.8 (0.813)	26.9 ± 16.6 (0.625)	13.7 ± 10.8 (1.000)	2.1 ± 0.6 (0.406)	1.6 ± 0.3 (0.094)
0.6	1389.9 ± 639.7 (1.000)	27.2 ± 17.3 (0.438)	15.6 ± 13.0 (1.000)	2.1 ± 0.6 (0.406)	1.6 ± 0.3 (0.063)
0.7	1401.0 ± 635.5 (0.625)	27.5 ± 17.2 (0.438)	15.7 ± 12.9 (0.813)	2.1 ± 0.6 (0.406)	1.6 ± 0.3 (0.063)
0.8	1402.7 ± 634.2 (0.625)	27.6 ± 17.2 (0.438)	16.7 ± 14.5 (0.813)	2.1 ± 0.6 (0.406)	1.6 ± 0.3 (0.063)
0.9	1416.0 ± 639.6 (0.625)	28.3 ± 17.5 (0.438)	17.0 ± 14.7 (0.625)	2.1 ± 0.6 (0.406)	1.6 ± 0.3 (0.063)
1.0	1418.0 ± 637.2 (0.625)	28.5 ± 17.3 (0.438)	17.1 ± 14.7 (0.625)	2.1 ± 0.6 (0.406)	1.6 ± 0.3 (0.063)
Average	1373.4 ± 552.8	26.3 ± 14.5	16.1 ± 13.1	2.1 ± 0.6	1.6 ± 0.3

The left lung cases showed no significant results for any of the investigated parameters as demonstrated in Table 2, although it should be noted that both average conformity indices are much lower for the algorithm-generated plans than the initial plans (5% and 16% improvements respectively).

Table 3: Mean ± standard deviation (and p-values) for all dosimetric parameters and values of k for right lung cases (significance level = 0.05).

k Value	Mean Lung Dose	V20 Lung	V40 Heart	Conformity (80%)	Conformity (90%)
Initial	1229.4 ± 417.6	19.8 ± 8.6	7.5 ± 4.5	2.2 ± 0.8	1.7 ± 0.6
0.1	1264.8 ± 510.2 (1.000)	23.2 ± 11.6 (0.187)	8.7 ± 7.2 (1.000)	2.1 ± 0.8 (0.031)	1.7 ± 0.6 (0.094)
0.2	1278.6 ± 524.7 (1.000)	23.0 ± 11.7 (0.312)	7.5 ± 6.1 (0.625)	2.0 ± 0.6 (0.063)	1.6 ± 0.5 (0.063)
0.3	1286.2 ± 521.0 (1.000)	23.6 ± 11.9 (0.188)	7.4 ± 6.0 (0.625)	2.0 ± 0.6 (0.031)	1.6 ± 0.4 (0.031)
0.4	1307.0 ± 522.3 (1.000)	23.6 ± 11.9 (0.125)	7.4 ± 5.9 (0.625)	1.9 ± 0.5 (0.031)	1.6 ± 0.4 (0.063)
0.5	1301.8 ± 530.1 (1.000)	23.9 ± 12.6 (0.313)	8.4 ± 7.5 (0.875)	2.1 ± 0.6 (0.031)	1.6 ± 0.5 (0.031)
0.6	1320.6 ± 550.2 (0.813)	24.0 ± 12.6 (0.313)	9.6 ± 9.8 (0.875)	2.0 ± 0.6 (0.031)	1.6 ± 0.5 (0.031)
0.7	1315.2 ± 554.4 (0.813)	24.0 ± 12.7 (0.313)	9.7 ± 9.9 (0.875)	2.0 ± 0.6 (0.031)	1.6 ± 0.5 (0.031)
0.8	1317.8 ± 552.8 (0.813)	24.1 ± 12.6 (0.313)	9.8 ± 9.9 (1.000)	2.0 ± 0.6 (0.031)	1.6 ± 0.5 (0.031)
0.9	1317.6 ± 550.9 (0.813)	24.1 ± 12.5 (0.313)	9.4 ± 9.3 (0.875)	2.0 ± 0.6 (0.031)	1.6 ± 0.5 (0.031)
1.0	1315.8 ± 547.9 (0.813)	24.0 ± 12.5 (0.313)	9.4 ± 9.3 (0.875)	2.0 ± 0.6 (0.031)	1.6 ± 0.5 (0.031)
Average	1302.5 ± 485.2	23.7 ± 11.1	8.7 ± 7.5	2.0 ± 0.6	1.6 ± 0.4

Unlike the left lung cases, the cases where the tumor is located in the right lung revealed significant results for the two conformity indices, as shown by Table 3. However, the results were not significant for all values of k, despite the average decrease of 14% in the 80% conformity index and 11% in the 90% conformity index.

Table 4: Mean ± standard deviation (and p-values) for all dosimetric parameters and values of *k* for mediastinum cases (significance level = 0.05).

k Value	Mean Lung Dose	V20 Lung	V40 Heart	Conformity (80%)	Conformity (90%)
Initial	1214.5 ± 377.4	22.2 ± 8.7	6.8 ± 7.0	2.6 ± 0.6	2.0 ± 0.5
0.1	1135.3 ± 369.9 (0.188)	19.8 ± 8.9 (0.063)	5.5 ± 6.0 (0.250)	2.4 ± 0.5 (0.031)	1.8 ± 0.3 (0.063)
0.2	1156.0 ± 359.6 (0.313)	19.9 ± 9.6 (0.063)	5.1 ± 5.5 (0.250)	2.3 ± 0.5 (0.031)	1.8 ± 0.3 (0.063)
0.3	1174.5 ± 368.4 (0.625)	20.7 ± 10.1 (0.313)	5.1 ± 5.7 (0.250)	2.3 ± 0.5 (0.156)	1.8 ± 0.3 (0.156)
0.4	1185.9 ± 340.7 (0.813)	21.0 ± 8.3 (0.313)	5.3 ± 5.7 (0.125)	2.3 ± 0.5 (0.031)	1.7 ± 0.3 (0.063)
0.5	1203.0 ± 343.4 (1.000)	22.0 ± 8.1 (1.000)	5.1 ± 6.1 (0.125)	2.2 ± 0.5 (0.031)	1.7 ± 0.3 (0.063)
0.6	1209.4 ± 338.1 (1.000)	22.0 ± 8.0 (1.000)	5.1 ± 6.1 (0.125)	2.2 ± 0.4 (0.063)	1.7 ± 0.2 (0.063)
0.7	1211.5 ± 337.7 (1.000)	22.1 ± 8.1 (1.000)	5.2 ± 6.1 (0.125)	2.2 ± 0.4 (0.063)	1.7 ± 0.3 (0.063)
0.8	1211.6 ± 337.8 (1.000)	22.1 ± 8.1 (1.000)	5.2 ± 6.1 (0.125)	2.2 ± 0.4 (0.063)	1.7 ± 0.3 (0.063)
0.9	1205.4 ± 346.1 (1.000)	22.1 ± 8.1 (1.000)	5.2 ± 6.1 (0.250)	2.3 ± 0.5 (0.156)	1.7 ± 0.3 (0.156)
1.0	1205.3 ± 346.1 (1.000)	22.1 ± 8.1 (1.000)	5.2 ± 6.1 (0.250)	2.3 ± 0.5 (0.313)	1.7 ± 0.3 (0.313)
Average	1189.8 ± 316.3	21.4 ± 7.8	5.2 ± 5.4	2.3 ± 0.4	1.7 ± 0.3

As with the other two tumor location groups, the p-values for all lung and heart parameters failed to prove significant for the mediastinum cases as shown in Table 4. Although, the conformity indices yet again show improvement in the algorithm-generated plans compared to the initial plans (12% and 13% improvements respectively), the signed-rank test reveals that only a handful of the *k* values provide significant results, and even then only for the 80% conformity index.

Comparing the three previous tables, it should be noted that while the majority of the parameters proved to be insignificant with regards to the Wilcoxon singed-rank test, this is likely due to the small sample size and all of the results can still be interpreted meaningfully.

The mean lung dose is noticeably lower and shows less variation in the mediastinum cases than in either the left or right lung cases, which should be expected considering that lateral beams would not be used to treat the mediastinum resulting in lower doses to the lungs. As with the previously presented results, the mean lung dose and V20 lung appear to be correlated as V20 lung is also lower in the mediastinum cases. The values of V40 heart are markedly higher in the left lung cases, which again should be expected because the heart will be closer to the PTV in these cases than the others.

4. Discussion

In order to be able to compare the 150 algorithm-generated plans with the 15 original clinical plans, many of the customizable parameters were kept constant. The OAR and PTV priorities, number of beams, and treatment technique (coplanar) were left identical for all plans. The beam angle separation parameter k was the only variable that was altered for each case, as the aim was to determine if an optimal value of this parameter exists.

4.1 Lung and Heart Dosimetry

The mean lung dose and V20 lung are both correlated with a risk of pneumonitis and loss of function as the parameter values increase. QUANTEC guidelines recommend limiting the mean lung dose to less than 24 Gy, and limiting V20 lung to less than 30% of the prescription [6, 19]. The parameter values from both the initial and algorithm-generated plans fall well below these thresholds, as evidenced by the measurements in Tables 1-4.

The V40 heart is correlated with a risk of pericarditis and risk of cardiac mortality with increasing dose. Recent studies suggest limiting V40 heart to less than 50% [21, 22]. With this in mind, it can be clearly seen again from the Tables 1-4 that the results of this study fall well within this limit.

Both when the patient cases were compared together and when they were broken into separate groups based on tumor location, the dosimetric parameters for the lungs and heart were not found to be statistically different from the initial plans. This implies that although the results may vary drastically from case to case (Figures 11-13), with some

producing markedly better measurements and others producing much worse compared to the initial plans, when considered as a whole, the distribution of the parameters shows no significant difference from that of the clinically treated plans. This large variation between cases is likely an effect of patient anatomy and tumor geometry since all other variables were purposefully kept constant.

Although ideally the dosimetric parameters from the algorithm-generated plans would show improvement over the initial plans, the fact that they have been proven to be similar instead of worse remains a positive result, because the automated method has the potential to drastically reduce the time-consuming aspect of the planning process while maintaining the same level of OAR sparing.

4.2 Conformity Indices

The conformity index is defined for any given isodose level as the volume enclosed by the isodose surface divided by the PTV volume (Equation 6). Based on this definition, under-dosing of the target would result in a conformity index less than one and over-dosing of the normal tissues would results in an index greater than one.

It is important to note that while a decrease in the conformity index is not necessarily an improvement because it can indicate under-dosing of the target, in this study all of the conformity indices (for both initial and algorithm-generated plans, and both 80% and 90% isodose levels) were always greater than one. Therefore, a decrease in the conformity index is desirable and should indeed be considered an improvement.

Given this, it is clear that the 11% reduction in the 80% conformity index and the 13% reduction in the 90% conformity index represent a significant improvement over the initials plans, especially when further compounded by the successful signed-rank analysis.

4.3 Optimal Beam Separation Value

The range of k values that were used in planning were chosen based on the fact that several of the dosimetric parameter values were noticed to saturate when large k values were attempted. Figures 11-15 show that for the majority of cases the dosimetric parameter values become constant in the range when $k > 0.8$ and even lower for some cases. In future work, it may be beneficial to investigate smaller k intervals in a more limited range.

Because none of the parameters had both correlation with k and significant differences in the algorithm-generated versus the initial plans, it can be inferred from the current data that a universally optimal value for this parameter does not exist. Alternatively, the beam separation parameter could be used to customize the automated planning process according to tumor geometry or intended outcome.

Below, Figure 18 shows a comparison between an initial plan and the corresponding algorithm-generated plan using the minimum beam separation parameter value. Both the initial and algorithm generated plans have very similar beam angle selections, which indicates that this type of case is best suited to a plan with a low value of k.

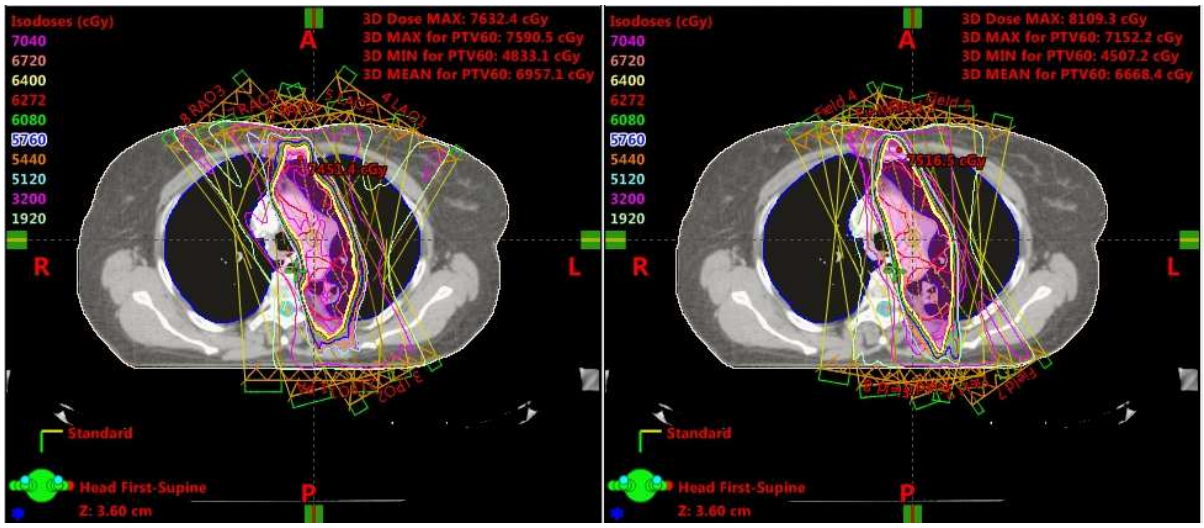

Figure 18: Comparison between an initial "low *k*" plan (left) and algorithm-generated plan where *k* = 0.1 (right).

Conversely, Figure 19 shows the same comparison between another initial plan and the corresponding algorithm-generated plan now using the maximum beam separation parameter value. In this example, the similar beam angle selections in both plans indicate that the most appropriate *k* value exists in the higher range.

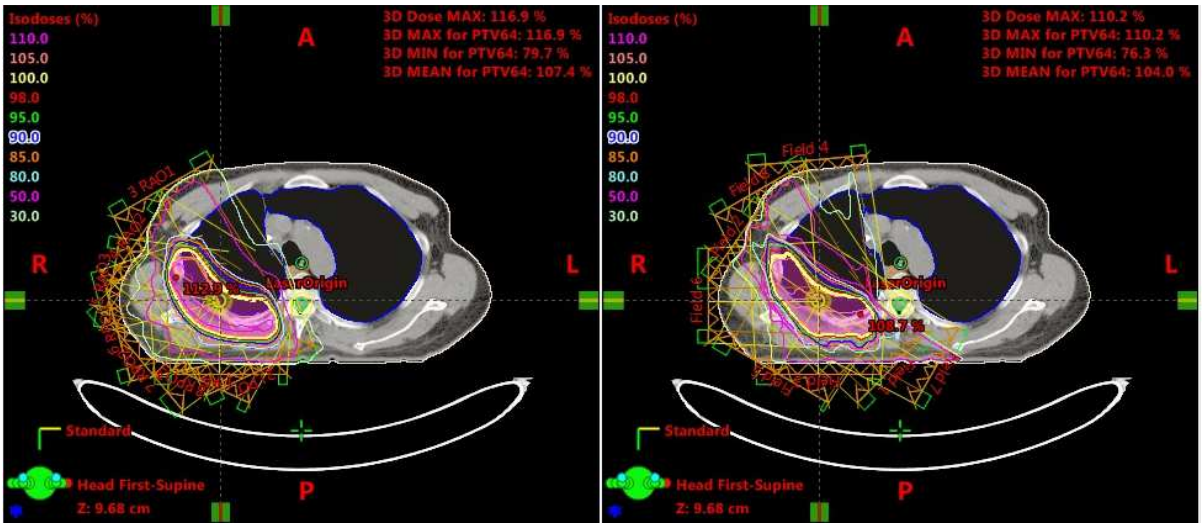

Figure 19: Comparison between an initial "high *k*" plan (left) and algorithm-generated plan where *k* = 1.0 (right).

From the remarkable similarities between the initial and algorithm-generated plans in the previous examples, it can be inferred that although a universally optimal *k* value does not exist, a most appropriate value may exist for certain case groups. In this study, tumor location was investigated, but found not to correspond with any particular beam separation parameter value; however, other factors may provide more conclusive results. Examining what may define these case groups is an option for future work, which is discussed in section 4.5.

4.4 Effect of Sample Size

Although some significant improvements of the algorithm-generated plans over the initial plans were noted, it is important to recognize that this investigation would have greatly benefitted from the inclusion of more patient cases. It is very possible that the trends (or apparent lack thereof) in the data could be the result of unintentional or unidentified

bias in the patient selection, and adding more patients would help eliminate this uncertainty and strengthen the conclusions drawn from this study. The analysis of plans based on tumor location was especially hindered by a simple lack of data.

4.5 Options for Future Work

Not only was this study only focused on half of the workflow for the proposed treatment planning automation method (Figure 6), but many of the customizable aspects of the beam angle selection algorithm were purposefully ignored in favor of investigating the beam separation parameter without the complication of potential interplay among the substantial number of variables. This leaves many potential avenues for further investigation and development

The individual OAR avoidance priorities could be examined to assess whether an ideal configuration of relative weights exists. A default configuration was used for the purposes of this study, but it is very possible that another configuration may results in higher quality plans. Altering the number of beams, or allowing non-coplanar angles would also likely have an effect on the algorithm's planning abilities. It would also be worthwhile to consider smaller intervals of the beam separation parameters, especially at low k values where the most variation was seen between data points. As mentioned previously, examining additional factors may reveal that an optimal k value indeed exists, if only for certain case groups.

Although there are many paths that could be explored to further this work, the greatest priority should be given to corroborating the current results with a larger patient set. It is also possible that with more cases included, the tumor location-specific results will reveal more meaningful trends or that the existing trends seen in the conformity indices will change.

5. Conclusion

To summarize, although this study would benefit from the inclusion of a larger dataset, the results obtained prove that this beam selection algorithm specifically and the IMRT automation method as a whole have merit and should be investigated further. Plans created with the automated method share similar dosimetric properties with minimal user input. The inclusion of the beam separation parameter noticeably improves dose conformity to the PTV with minimal effect on OAR and normal tissue sparing. Future work should be concentrated on verifying results with more patient cases and investigating the other algorithm variables.

References

1. Key Statistics for Lung Cancer." *Key Statistics for Lung Cancer*. Web. 16 Mar. 2016.

2. Dobbs, Jane, and Ann Barrett. "Practical radiotherapy planning." (1985).

3. Khan, Faiz M., and John P. Gibbons. *Khan's the Physics of Radiation Therapy*. Lippincott Williams & Wilkins, 2014.

4. Van Dyk, Jake. *The Modern Technology of Radiation Oncology: A Compendium for Medical Physicists and Radiation Oncologists*. Medical Physics Pub Corp, 1999.

5. Memorial Sloan-Kettering Cancer Center. *A Practical Guide to Intensity-Modulated Radiation Therapy*. Medical Physics Publishing Corporation, 2003.

6. Marks, Lawrence B., et al. "Use of normal tissue complication probability models in the clinic. "*International Journal of Radiation Oncology* Biology* Physics* 76.3 (2010): S10-S19.

7. Pugachev, Andrei, et al. "Role of beam orientation optimization in intensity-modulated radiation therapy." *International Journal of Radiation Oncology* Biology* Physics* 50.2 (2001): 551-560.

8. Das, Shiva, et al. "Beam orientation selection for intensity-modulated radiation therapy based on target equivalent uniform dose maximization."*International Journal of Radiation Oncology* Biology* Physics* 55.1 (2003): 215-224.

9. Li, Yongjie, Jonathan Yao, and Dezhong Yao. "Automatic beam angle selection in IMRT planning using genetic algorithm." *Physics in medicine and biology* 49.10 (2004): 1915.

10. Wang, Xiaochun, et al. "Effectiveness of noncoplanar IMRT planning using a parallelized multiresolution beam angle optimization method for paranasal sinus carcinoma." *International Journal of Radiation Oncology* Biology* Physics*63.2 (2005): 594-601.

11. Jia, Xun, et al. "Beam orientation optimization for intensity modulated radiation therapy using adaptive l2, 1-minimization." *Physics in medicine and biology* 56.19 (2011): 6205.

12. Zhang, H. H., et al. "A surrogate-based metaheuristic global search method for beam angle selection in radiation treatment planning."*Physics in medicine and biology* 58.6 (2013): 1933.

13. Breedveld, Sebastiaan, et al. "iCycle: Integrated, multicriterial beam angle, and profile optimization for generation of coplanar and noncoplanar IMRT plans." *Medical physics* 39.2 (2012): 951-963.

14. Schreibmann, Eduard, and Lei Xing. "Feasibility study of beam orientation class-solutions for prostate IMRT." *Medical physics* 31.10 (2004): 2863-2870.

15. Meyer, J., S. M. Hummel, P. S. Cho, M. M. Austin-Seymour and M. H. Phillips (2005). "Automatic selection of non-coplanar beam directions for three-dimensional conformal radiotherapy." Br J Radiol 78(928): 316-327.

16. Abraham, Christophe, Nicolas Molinari, and Rémi Servien. "Unsupervised clustering of multivariate circular data." *Statistics in medicine* 32.8 (2013): 1376-1382.

17. Zhang, Xiaodong, et al. "A methodology for automatic intensity-modulated radiation treatment planning for lung cancer." *Physics in medicine and biology* 56.13 (2011): 3873.

18. Yuan, Lulin, et al. "Quantitative analysis of the factors which affect the interpatient organ-at-risk dose sparing variation in IMRT plans." *Medical physics* 39.11 (2012): 6868-6878.

19. Marks, Lawrence B., et al. "Radiation dose–volume effects in the lung." *International Journal of Radiation Oncology* Biology* Physics* 76.3 (2010): S70-S76.

20. Gagliardi, Giovanna, et al. "Radiation dose–volume effects in the heart." *International Journal of Radiation Oncology* Biology* Physics* 76.3 (2010): S77-S85.

21. Cosset, J. M., et al. "Pericarditis and myocardial infarctions after Hodgkin's disease therapy."*International Journal of Radiation Oncology* Biology* Physics* 21.2 (1991): 447-449.

22. Van Cutsem, E., et al. "Efficacy results from the ToGA trial: a phase III study of trastuzumab added to standard chemotherapy in first-line HER2-positive advanced gastric cancer." *J Clin Oncol* 27 (2009): 15s.